External Field Coupling to MTL Networks with Nonlinear Junctions: Numerical Modeling and Experimental Validation

Tibor Lapohos, *Member, IEEE,* Joe LoVetri, *Member, IEEE,* and Joe Seregelyi, *Member, IEEE*

***Abstract*—The problem of predicting the voltages and currents induced on a printed circuit multiconductor transmission line (MTL) network by an impinging transient plane wave electromagnetic field is considered. The MTL network contains nonlinear circuit elements and test cases with various dielectric substrates are examined. Numerical predictions based on quasi-TEM models of the MTL's and modified nodal analysis (MNA) models of the lumped element junctions are compared to experimental results obtained in the time domain using a GTEM cell. As has been done in the past, the effect of the incident plane wave is introduced as forcing functions in the MTL equations. The primary goal of this paper is to *quantify* the accuracy of the various commonly used quasi-TEM mathematical time-domain models. It is shown that when modeling the forcing function terms, it is important to take into account the perturbation of the incident plane wave due to the dielectric substrate. (The experimental-numerical comparisons herein are shown for the case of end-fire illumination since it best demonstrates this point.) Neglecting the dielectric effect on the incident transient pulse, even for substrates with low dielectric constant, produces poor results.**

***Index Terms*—Experimental validation, field coupling, measurements, modified nodal analysis, modeling, MNA, MTL, MTL network, nonlinear circuits, printed circuit board, surface wave, transient.**

I. Introduction

VARIOUS models exist for predicting the induced voltages and currents produced by the coupling of electromagnetic waves into a multiconductor transmission-line (MTL) network. The more accurate of these are formulated as three-dimensional (3-D) electromagnetic field problems. Voltages and currents are then obtained from the solution of the field quantities. The task of trying to include extensive nonlinear lumped element circuits to these field models in a manner amenable to efficient computer solution is still an area of investigation. Various examples of solving an electromagnetic field problem in the presence of modestly sized nonlinear circuits do exist in the literature (see [1] and [2] for example), but the techniques used in these investigations would require great computational resources if applied to practical sized printed circuit board problems. In the present work, the specific case of modeling printed circuit board (PCB) MTL networks with nonlinear junctions is considered.

Manuscript received February 17, 1998; revised November 16, 1999.

T. Lapohos and J. Seregelyi are with the Department of National Defence, Defence Research Establishment Ottawa, Ottawa, ON, K1A 0Z4 Canada.

J. LoVetri is with the Department of Electrical and Computer Engineering, University of Manitoba, Winnipeg, Manitoba, Canada R3T 5V6.

Publisher Item Identifier S 0018-9375(00)2182-7.

For practical problems, it is common to use distributed circuit models of MTL networks due to their simplicity of formulation and the fact that computer solutions can be obtained more efficiently than full field solutions. Although various distributed circuit models exist, such as the partial element equivalent circuit (PEEC) [3], simply using a quasi-TEM formulation of the MTL's and a lumped element formulation of the junctions has provided reasonable results for many applications [4]. Starting from the quasi-TEM formulation, efficient model order-reduction techniques based on the asymptotic waveform evaluation (AWE) technique have been implemented for relatively large problems [5]. The quasi-TEM formulation is also the basis of approximate SPICE models which have been developed in the past [4], [6]–[8]. The existence of an external field coupling to the MTL's can be introduced into the model as distributed voltage and current sources along the line [4], [9]–[11] and these manifest themselves as forcing function terms in the MTL equations. Many techniques have been reported for solving these now inhomogeneous partial differential equations (see for instance [12]).

In [13], the authors have pointed out the importance of incorporating the effect of the dielectric layer in the field coupling model. Their frequency domain derivations are valid for a finite size conducting strip embedded in a thin dielectric substrate of infinite extent. This configuration is exposed to a plane wave illumination. The same authors present a more general case [14] using a full-wave model. This time the source of the external field is a dipole with an arbitrary orientation. The work is highly encompassing, taking into account several aspects of the problem. Unfortunately, the possibility of including nonlinear terminal conditions in this formulation seems very difficult. The works presented in [15] and [16] also make use of full-field analytical models to determine the field coupling to a printed two wire line. It was pointed out in [17] that significant differences between simulations based on the quasi-TEM MTL model and full wave finite-difference time-domain (FDTD) simulations or measurements can be expected due to the fact that the quasi-TEM MTL model does not incorporate the finite length of the conducting strips. It has been shown that assuming infinite length for finite length strips results in underestimation of the peak voltage and current values induced by the external fields.

In this paper, we use the quasi-TEM formulation for the MTL's and a modified nodal analysis (MNA) formulation of the possibly nonlinear lumped-element junctions between MTL's. Then the complete system, including the MNA equations, is solved in the time domain using finite-difference techniques.

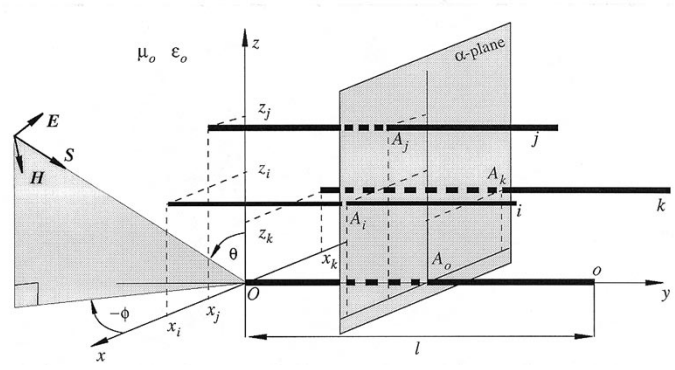

Fig. 1. MTL illuminated by an electromagnetic plane wave.

The technique used herein is similar to that reported in [18]. Since we are considering printed circuit MTL networks, in order to accurately model the field in the dielectric substrate we use a 3-D [for certain particular cases, two-dimensional (2-D)] FDTD technique [20]. The advantage of this method lies in the fact that it accurately models the incident coupling field, but this full field analysis needs to be carried out only once and on a much simpler problem consisting of only the PCB dielectric layers (i.e., no traces and no electronic components). As such, the method can be applied in practical PCB design and EMC analysis procedures. Simulation results obtained using this technique, as well as those making the approximation that the incident plane wave remains a pure plane wave in the dielectric, are compared to measurements. Before describing this method and detailing the experimental and simulation results, a brief summary of the quasi-TEM formulation and the numerical technique for solving the MTL network equations is given.

II. Quasi-TEM Formulations of MTL's

Assuming a quasi-TEM mode of propagation along an MTL consisting of $m+1$ conductors (see Fig. 1), the time-dependent voltages $\boldsymbol{V}(t, y)$ and currents, $\boldsymbol{I}(t, y)$ along the conductors can be modeled by the following system of coupled partial differential equations:

$$\begin{cases} \dfrac{\partial}{\partial y}\boldsymbol{V}(t, y) + L\dfrac{\partial}{\partial t}\boldsymbol{I}(t, y) + R\boldsymbol{I}(t, y) = \boldsymbol{V}_f(t, y) \\ \dfrac{\partial}{\partial y}\boldsymbol{I}(t, y) + C\dfrac{\partial}{\partial t}\boldsymbol{V}(t, y) + G\boldsymbol{V}(t, y) = \boldsymbol{I}_f(t, y) \end{cases} \tag{1}$$

where L, C, R, and G denote the per-unit-length (PUL) inductance, capacitance, resistance, and conductance $m \times m$ matrices, respectively. The $m \times 1$ vector forcing functions $\boldsymbol{V}_f(t, y)$ and $\boldsymbol{I}_f(t, y)$ represent the distributed voltages and distributed currents that are due to the impinging external electromagnetic field. These can be expressed in three completely equivalent formulations [11]: 1) in terms of incident transverse electric and magnetic fields [9]; 2) in terms of only the incident electric field [10]; and 3) in terms of only the incident magnetic field [11]. Only the first formulation uses total voltages and currents and, although these forcing terms are more complicated than those of the latter two formulations, using total voltages and currents simplifies the interface to the lumped element formulation of the MTL junctions. In this formulation, the forcing functions are given by (2) below where in the line integral terms A_j denotes the point at which the α-plane, which is perpendicular to the y-axis, intersects the jth line of the MTL as shown in Fig. 1. The α-plane intersects the y-axis (which is colinear with the reference conductor zero) at point A_0 whose coordinates are (0, y, 0). In (2), shown at the bottom of the page, $\boldsymbol{E}_t^i$ denotes the transverse component of the incident electric field intensity vector $\boldsymbol{E}^i$, which is the projection of $\boldsymbol{E}^i$ onto the α-plane. The magnitude of the longitudinal component of the incident electric field is denoted by $\boldsymbol{E}_y^i$.

In the above definitions of the forcing functions, the incident field is defined as that which would exist if all the conductors of the MTL were removed. This implies that in order to accurately model the distributed sources, this incident field must be determined as accurately as possible. This type of coupling model, that is for the particular case of plane wave incidence, has been investigated extensively in the literature. However, when modeling printed circuit board MTL networks, a typical approximation that is made is to ignore the perturbation of the incident plane wave due to the dielectric substrate of the circuit board. In this paper, by comparing various test cases with experimental results, we show that such approximations can lead to completely erroneous results.

III. Finite Difference Solution of the MTL/MNA Model

We discretize the MTL equations (1) by using an interlaced leap-frog scheme such that the currents are evaluated at half-time steps and half-spatial positions, whereas the voltages are evaluated at integer-time steps and integer-spatial positions; that is

$$\boldsymbol{I}_{k+1/2}^{n+1/2} \cong \boldsymbol{I}((n+1/2)\Delta t,\ (k+1/2)\Delta y), \quad k = 0 \cdots K-1,\ n = 1, 2, 3, \cdots \tag{3}$$

$$\begin{cases} \boldsymbol{V}_f(t, y) = \begin{bmatrix} \cdots \\ -\dfrac{\partial}{\partial y}\displaystyle\int_{A_0}^{A_j} \boldsymbol{E}_t^i \cdot \boldsymbol{dl} + E_y^i(t, x_j, y, z_j) - E_y^i(t, 0, y, 0) \\ \cdots \end{bmatrix} \\ \boldsymbol{I}_f(t, y) = -G\begin{bmatrix} \cdots \\ \displaystyle\int_{A_0}^{A_j} \boldsymbol{E}_t^i \cdot \boldsymbol{dl} \\ \cdots \end{bmatrix} - C\dfrac{\partial}{\partial t}\begin{bmatrix} \cdots \\ \displaystyle\int_{A_0}^{A_j} \boldsymbol{E}_t^i \cdot \boldsymbol{dl} \\ \cdots \end{bmatrix} \end{cases} \tag{2}$$

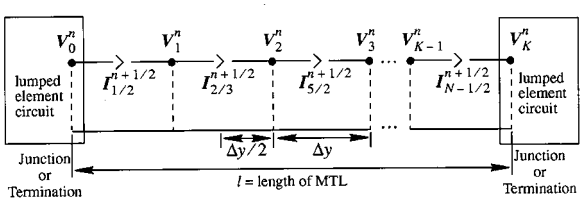

Fig. 2. The Π-model of a multiconductor TL.

$$\boldsymbol{V}_k^n \cong \boldsymbol{V}(n\Delta t,\, k\Delta y), \qquad k = 0 \cdots K,\, n = 1, 2, 3, \cdots. \tag{4}$$

This discretization corresponds to a Π-model of the line, as illustrated in Fig. 2. It is now a simple procedure to find the following update equations for all the currents and the interior voltages along the line [4] in (5), shown at the bottom of the page. We keep the discretized distributed voltage and current sources $[\boldsymbol{V}_f]_{k+1/2}^n$ and $[\boldsymbol{I}_f]_k^{n+1/2}$ in a simple notational form since it is their treatment in which the models discussed herein differ from each other.

The solutions of the lumped element circuits at junctions between MTL's or at the termination of an MTL are formulated using MNA [19]. The specific technique used is similar to that reported in [18] except that here we use a Π-model of the MTL and in that work the T-model was used. The effect is that in the T-model, the MTL voltages one-half cell away from the terminations of the line are included as known sources in the MNA formulation, whereas in the Π-model, the MTL currents one-half cell away from the terminations of the line are included as sources in the MNA formulation. In some cases, this procedure reduces the size of the MNA matrix significantly. As in [18], the nonlinear circuits are solved using a Newton–Raphson algorithm. In all the nonlinear numerical examples presented in this paper the MNA equations are solved using this algorithm.

IV. Field Coupling Terms of the MTL Equations

As has been pointed out in Section I, a frequently employed approximation when evaluating the *exact* forcing functions (2) of the quasi-TEM MTL equations (1) is to assume that, in the case of a plane wave illuminating *source*, the incident field in the immediate proximity of the conductor elements of the MTL's is also planar. The primary goal of this paper is to show, using comparisons with experimental data, that this approximation may lead to inaccurate results even for the simple but common case of a single dielectric layer PCB. In this section, two versions of the discretized forcing terms for the MTL equations are developed. The first assumes a purely plane wave incident field, while the second allows us to insert any form of discretized incident field. These are referred to as the "plane wave" or "nonplane wave" models, respectively.

A. Plane Wave Field Coupling Models

Consider an transient electromagnetic plane wave, which is propagating in the $-\hat{a}_r$ unit direction of a spherical coordinate system (r, θ, ϕ) when θ and ϕ are specified constant angles. The wave is propagating in free space with propagation velocity $\boldsymbol{v} = -v_0\hat{a}_r = v_x\hat{a}_x + v_y\hat{a}_y + v_z\hat{a}_z$, where $v_0 = (\mu_0\varepsilon_0)^{-1/2}$. At any position in space, given by the Cartesian coordinates (x, y, z), the electric field of the incident plane wave can be specified as

$$\boldsymbol{E}^i(t, x) = \boldsymbol{e}E_0(t - (\boldsymbol{v}\cdot\boldsymbol{x})/v_o^2) \tag{6}$$

where $\boldsymbol{x} = x\hat{a}_x + y\hat{a}_y + z\hat{a}_z$ is the position vector and $\boldsymbol{e} = e_x\hat{a}_x + e_y\hat{a}_y + e_z\hat{a}_z$ is the unit vector defining the polarization of the electric field at that point. The waveform (in space or time) of the field is defined by the function $E_0(\cdot)$. Explicit expressions for the forcing functions $\boldsymbol{V}_f(t, y)$ and $\boldsymbol{I}_f(t, y)$ can be found by first converting the original forcing functions to the phasor domain, carrying out some analytic manipulations, making the approximation that the wavelength is large as compared to the distance between conductors, and subsequently converting back to the time domain. The complete procedure is described in [4] and, employing the present notation, the forcing functions can be written as

$$\begin{cases} \boldsymbol{V}_f(t, y) = \begin{bmatrix} \cdots \\ \left(\dfrac{f_j}{g_j}v_y - e_y\right)\dfrac{g_j}{v_0^2} \\ \cdots \end{bmatrix} \dfrac{\partial}{\partial t}E_0(t - v_y y/v_0^2) \\ \boldsymbol{I}_f(t, y) = -C\begin{bmatrix} \cdots \\ f_j \\ \cdots \end{bmatrix} \dfrac{\partial}{\partial t}E_0(t - v_y y/v_0^2) \end{cases} \tag{7}$$

where

$$\begin{cases} f_j = e_x x_j + e_z z_j \\ g_j = v_x x_j + v_z z_j \end{cases}, \qquad \forall\, j. \tag{8}$$

Except for a constant multiplicative factor that depends on the specific conductor, the time and space variation of the forcing functions is the same for all conductors of the MTL. The large wavelength approximation that has been used is nothing exceptional since it is a basic requirement for the quasi-TEM formulation of the MTL equations in the first place.

The forcing functions given by (7) are now discretized using a second-order accurate finite difference scheme and we arrive

$$\begin{cases} \boldsymbol{I}_{k+1/2}^{n+1/2} = \left[\Delta y\left(\dfrac{L}{\Delta t} + \dfrac{R}{2}\right)\right]^{-1}\left[\Delta y\left(\dfrac{L}{\Delta t} - \dfrac{R}{2}\right)\boldsymbol{I}_{k+1/2}^{n-1/2} - \boldsymbol{V}_{k+1}^n + \boldsymbol{V}_k^n + \Delta y[\boldsymbol{V}_f]_{k+1/2}^n\right] \\ \boldsymbol{V}_k^{n+1} = \left[\Delta y\left(\dfrac{C}{\Delta t} + \dfrac{G}{2}\right)\right]^{-1}\left[\Delta y\left(\dfrac{C}{\Delta t} - \dfrac{G}{2}\right)\boldsymbol{V}_k^n - \boldsymbol{I}_{k+1/2}^{n+1/2} + \boldsymbol{I}_{k-1/2}^{n+1/2} + \Delta y[\boldsymbol{I}_f]_k^{n+1/2}\right] \end{cases} \tag{5}$$

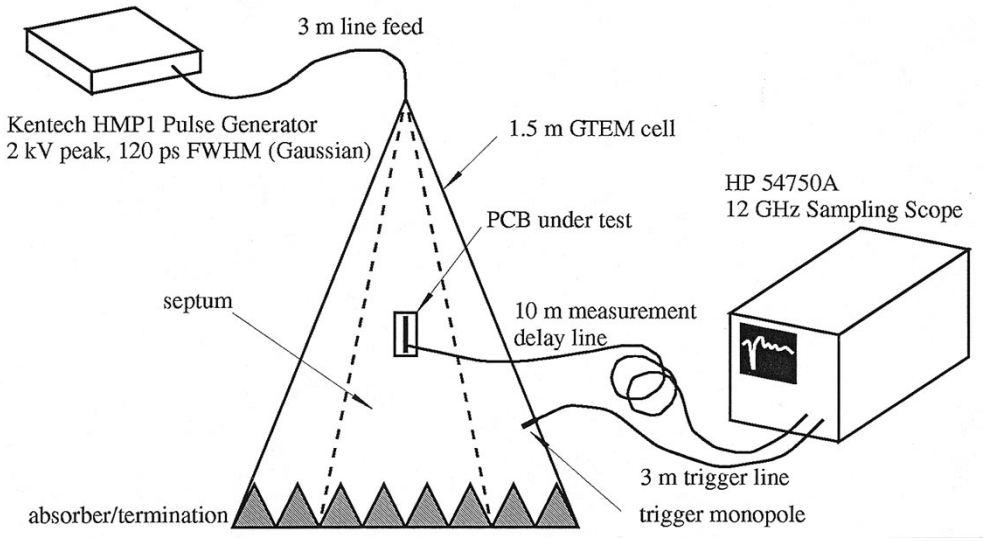

Fig. 3. Instrumentation setup used for the experimental validation of the field-to-MTL coupling models.

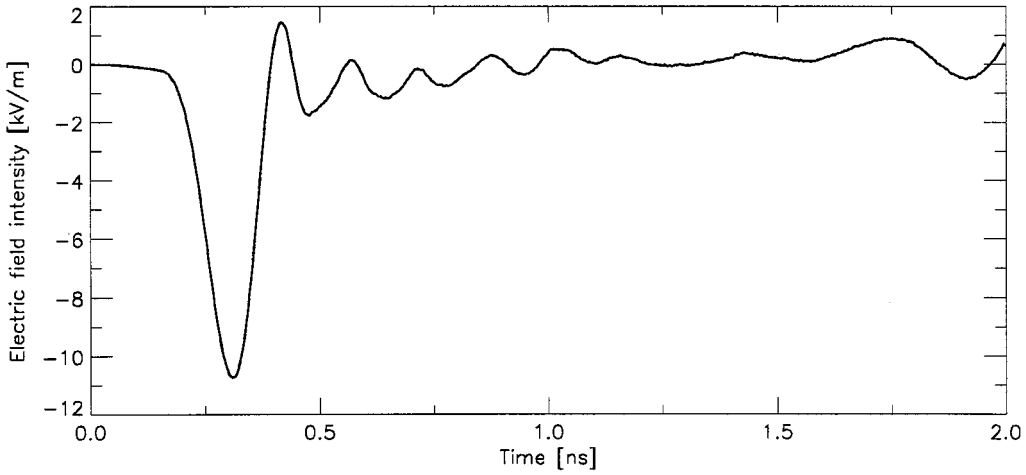

Fig. 4. The measured waveform of the incident electric field.

at the discrete form forcing functions in (9), shown at the bottom of the page, where

$$[E_a]_k^n = E_0(n\Delta t - v_y k\Delta y/v_0^2).$$

Equations (5) and (9) represent the simplified plane wave field coupling problem.

B. Nonplane Wave Field Coupling Models

The discrete form of the forcing functions as represented by (9) are approximations which inherently assume a plane wave incident on the MTL. These are very efficient to implement and need to be only slightly modified when a ground plane exists [4]. If the true incident field is not a plane wave then one could ignore this fact and continue to use (9) or one could determine

$$\begin{cases} [\boldsymbol{V}_f]_{k=1/2}^n = \begin{bmatrix} \cdots \\ \left(\dfrac{f_j}{g_j} v_y - e_y\right) \dfrac{g_j}{v_0^2} \\ \cdots \end{bmatrix} \dfrac{[E_a]_{k+1/2}^{n+1/2} - [E_a]_{k+1/2}^{n-1/2}}{\Delta t} \\ [\boldsymbol{I}_f]_k^{n+1/2} = -C \begin{bmatrix} \cdots \\ f_j \\ \cdots \end{bmatrix} \dfrac{[E_a]_k^{n+1} - [E_a]_k^n}{\Delta t} \end{cases} \tag{9}$$

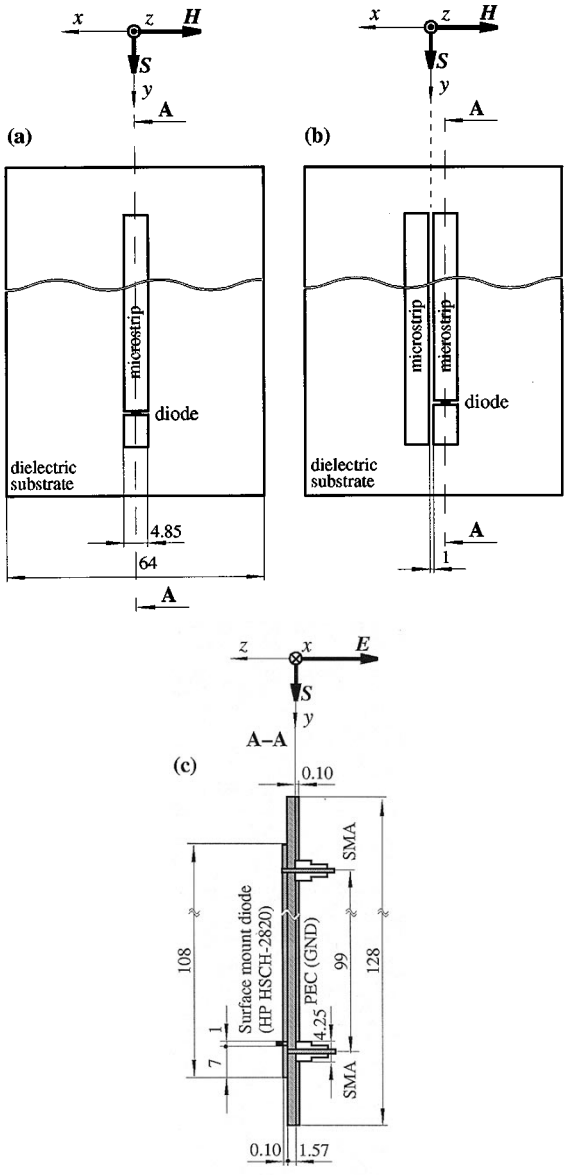

Fig. 5. Geometric layout of the (a) single and (b) coupled microstrips and (c) their cross-sectional view, including the relative orientation of the plane wave incidence.

the discretized forcing functions $\boldsymbol{V}_f(t, y)$ and $\boldsymbol{I}_f(t, y)$ by discretizing directly the integral terms (2) with the appropriate incident field inserted.

It is well known that heterogeneities in the proximity of the MTL conductors, such as the dielectric substrate, distort the external field and can give rise to *surface waves*, which are guided by the air-substrate interface. The above plane wave model obviously disregards these surface waves since, when it comes to the external field coupling, it assumes free-space in the proximity of the MTL conductors; the heterogeneities are modeled only through the PUL parameters of the MTL. In the case of a circuit board, the true impinging waveform is far more complicated than a pure plane wave. The actual waveform is a nontrivial function of position along the TL. This complicated waveform can be handled by the PDE formulation of the MTL's but, currently, no technique for incorporating this waveform into the SPICE implementable models is known.

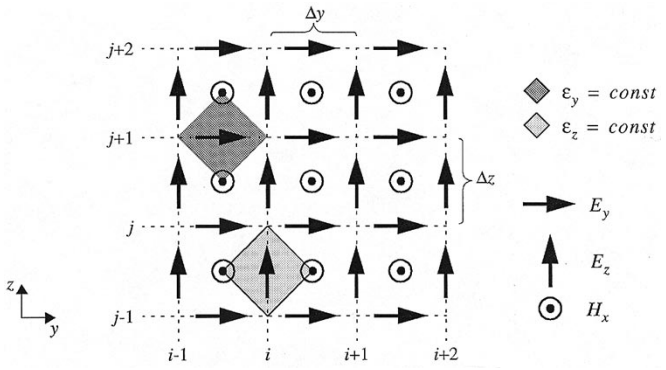

Fig. 6. Visualization of the 2-D FDTD computation cells.

In this paper, the field quantities necessary to evaluate the integral terms of (2) are obtained by using an FDTD analysis of the MTL structure carried out in the absence of the conductors themselves. The advantage of this procedure over using a 3-D full-field analysis of the entire MTL network lies in the fact that the expensive calculation of the field coupling to the MTL network has to be carried out only once for a given plane wave excitation; using the so-obtained database any number of simulations of different networks can be done for the same substrate. This is a computational time-saving procedure, which can be applied in PCB design effectively.

The forcing functions given by (2) can be discretized as

$$\begin{cases} [V_f]_{k+1/2}^n = -\dfrac{[S_t^j]_{k+1}^n - [S_t^j]_k^n}{\Delta y} + [S_l^j]_{k+1/2}^n \\ [\boldsymbol{I}_f]_k^{n+1/2} = -G\dfrac{[S_t^j]_k^{n+1} + [S_t^j]_k^n}{2} - C\dfrac{[S_t^j]_k^{n+1} - [S_t^j]_k^n}{\Delta t} \end{cases} \tag{10}$$

where the notation

$$\begin{cases} S_t^j = \displaystyle\int_{A_0}^{A_j} \boldsymbol{E}_t^i \cdot \boldsymbol{dl} \\ S_l^j = E_y^i(t, x_j, y, z_j) - E_y^i(t, 0, y, 0) \end{cases} \tag{11}$$

has been introduced for simplicity. The integral term in (11) can be easily evaluated numerically by using discrete field values from an FDTD or other numerical analysis of the PCB with all conductors removed.

Apparently, the need for an FDTD, or other full-field, solver is the only disadvantage of this approach. An analytical solution of the fields inside the substrate of finite size would be an optional choice. As already mentioned in Section I, the authors of [15] and [16] calculate the incident field analytically but assume a substrate of infinite extent. Based on the conclusions of [17], the accuracy of their assumption remains to be verified. The work reported in [21] shows that a direct relationship exists between the incident field (with all conductors and dielectric removed) and the forcing functions of the total field formulation of the quasi-TEM MTL equations. Unfortunately, a key step in that procedure involves the solution of an integral equation in order to calculate a vector multiplicative constant. However, this has

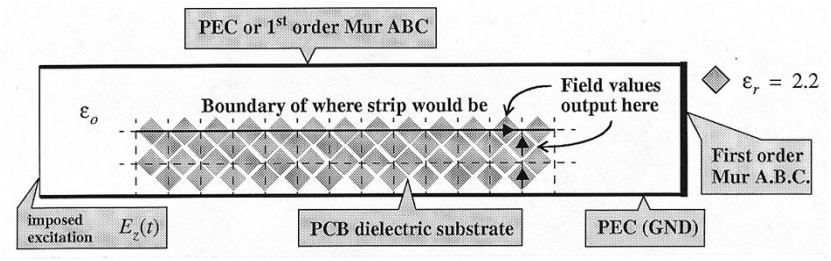

Fig. 7. Discretization of the substrate dielectric for the calculation of the "true" incident electric field.

to be done only once for uniform lines, so it could be an option for computing the fields required in (11).

V. Comparison of Experimental/Numerical Results

A. The Experimental Setup and the PCB Design

In order to evaluate the accuracy of the field-to-MTL coupling models, measurements were made for the case of PCB MTL's illuminated by a plane wave. The measurements were made using the instrumentation setup shown in Fig. 3. As the figure shows, the 1.5-m-high GTEM cell is fed from a Kentech[1] pulse generator. This generator produces 2-kV quasi-Gaussian pulses of 120 ps width. As a result, the peak value of the electric field inside the GTEM cell is approximately 10 kV/m. The microstrip structures are mounted on the access port of the GTEM cell. A monopole mounted on the side wall of the GTEM cell is used to generate the triggering signal for the oscilloscope. The signal induced on the microstrip was sampled using an SMA connector as a probe beneath the microstrip. The connection from the SMA connectors of the studied PCB's to the 12-GHz oscilloscope was made using a 10-m-long coaxial cable in order to assure a time delay with respect to the triggering signal, which is fed to the scope through a short (3 m) coaxial cable.

The transfer function of the probe-cable assembly was measured in order to calibrate the system. The inverse of this transfer function was used to scale all recorded measurement data collected from the PCB's. The same procedure was applied at the feedpoint of the GTEM cell. The waveform displayed in Fig. 4 is a sample of the electric field at the middle of the TL. It is important to mention that, since the GTEM cell is tapered, there is approximately a 15% reduction in field strength along the length of the microstrip. Hence, the SMA probe excitation at the back of the line will be proportionally smaller than at the front of the line. It should also be noted that the very small reflection from the termination of the cell occurs outside of the time window shown in all the measurements.

Several PCB's were used in the experiments. While maintaining the same basic structure, the substrate material and certain microstrip dimensions were varied. Two- and three-conductor microstrip structures with various linear and nonlinear terminations were studied. Since all the considered types of dielectric substrate materials produced similar results, we present only those obtained for the RT/duroid 5880 ($\varepsilon_r \cong 2.2 \pm 0.02$).[2]

[1]Kentech Instruments Ltd., Unit 9, Hall Farm Workshops, Oxon, UK, OX11 9AG, Tel. (+44) 235–510–748.

[2]RT/duroid 5880 ($\varepsilon_r = 2.20 \pm 0.02$) and TMM-4 ($\varepsilon_r = 4.50 \pm 0.045$) are manufactured by Rogers Corp., 100 S. Roosevelt Ave., Chandler, AZ 85226.

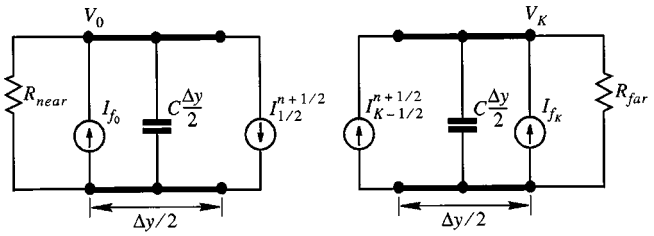

Fig. 8. Near- and far-end Thévenin termination circuits of a Π-modeled two-conductor lossless TL illuminated by an external field.

The details of the PCB's and their orientation with respect to the illuminating plane wave are shown in Fig. 5. Due to limitations in how the PCB's could be mounted onto the access port of the GTEM cell, only the depicted end-fire excitation case was studied. Nevertheless, the end-fire excitation produces the largest surface wave component, it is the best test case to investigate the limitations of using a simple plane wave coupling model. Also, in order to achieve the highest possible peak values of the induced pulses in the MTL's, a vertical polarization of the electrical field was chosen.

All PCB's incorporated a ground plane as the reference conductor. The geometric layout of the simplest two-conductor TL that was used is shown in Fig. 5(a). The SMA connectors were spaced symmetrically under the conducting strip as shown in Fig. 5(c). The overhang of the strip above its contact points with the SMA connectors assures that a good impedance match is made.

For the single microstrip case, the PUL parameters are calculated as $C = 914$ pF/m and $L = 229$ nH/m, hence having a characteristic impedance of $Z_c = 50\ \Omega$. The characteristic impedance was chosen to be 50 Ω in order to match the 50-Ω measurement system. The geometric layout of the dual microstrip is shown in Fig. 5(b). The PUL parameters of this structure were calculated as

$$C \cong \begin{bmatrix} 93.587 & -11.045 \\ -11.045 & 93.587 \end{bmatrix} \text{ pF/m}$$

and

$$L \cong \begin{bmatrix} 225.98 & 40.319 \\ 40.319 & 225.98 \end{bmatrix} \text{ nH/m.}$$

B. 2-D FDTD Evaluation of Incident Field

Since the TL's were exposed only to end-fire excitation, a simple 2-D FDTD field computation was used to evaluate the incident electric field inside the dielectric substrate. These field values were then used in (11) to evaluate the forcing functions.

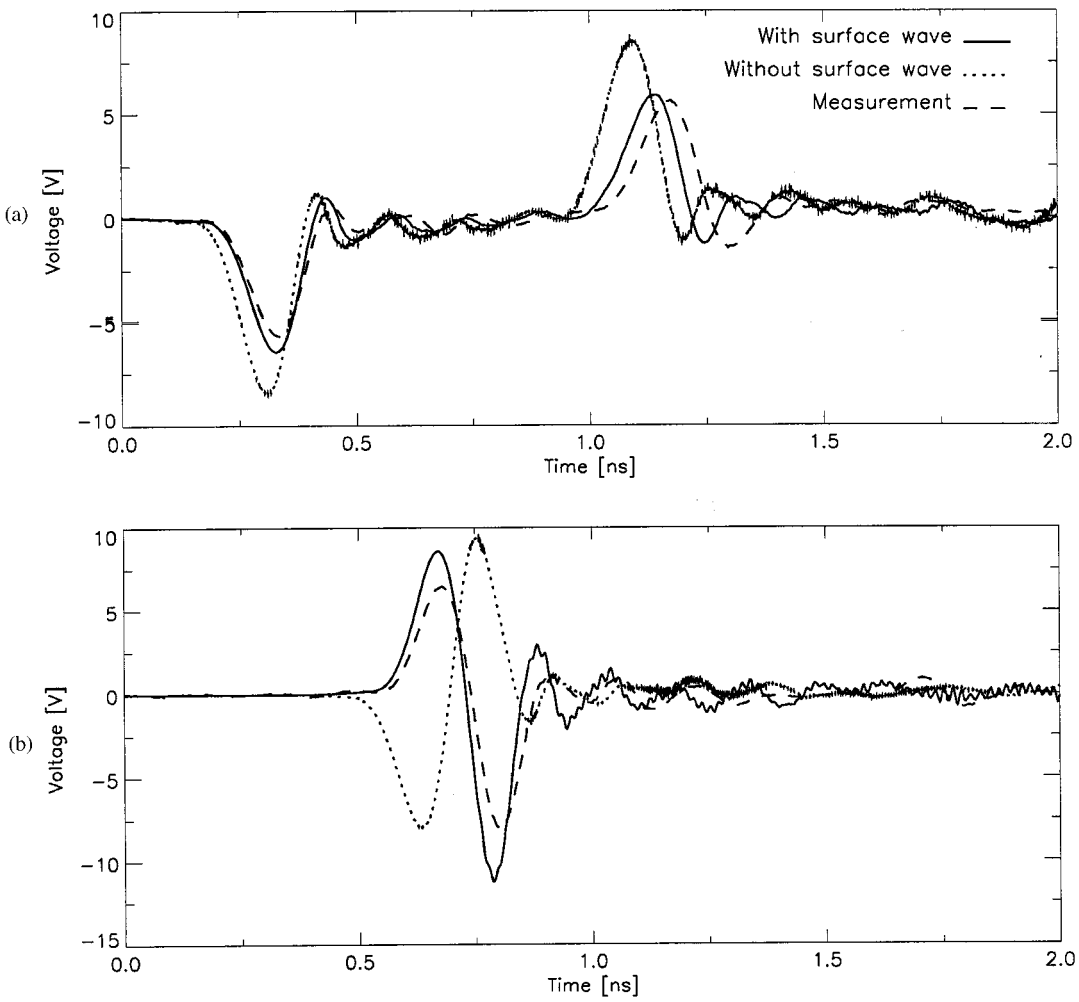

Fig. 9. Comparison of the plane wave model, surface wave (FDTD) model, and measurement results at the (a) near end and (b) far end of the two conductor TL.

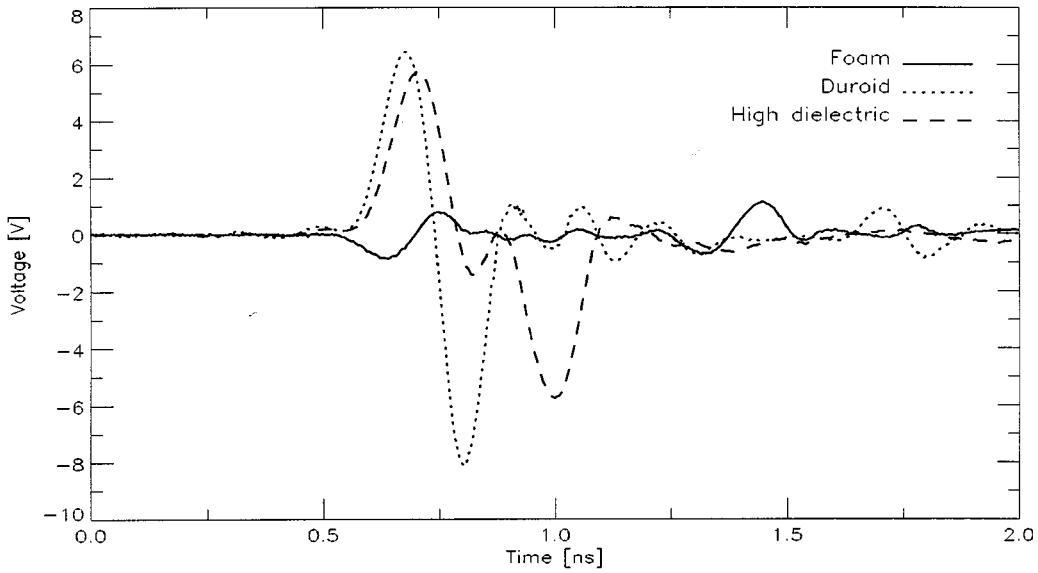

Fig. 10. The external field to TL coupling mechanism at the far-end for various substrates.

We use the well-known 2-D FDTD technique [20] to solve for the $\boldsymbol{E}_y$, $\boldsymbol{E}_z$, $\boldsymbol{H}_x$ electromagnetic field components on the time-space interlaced computational mesh shown in Fig. 6. Using this method one can specify permittivity values only on the

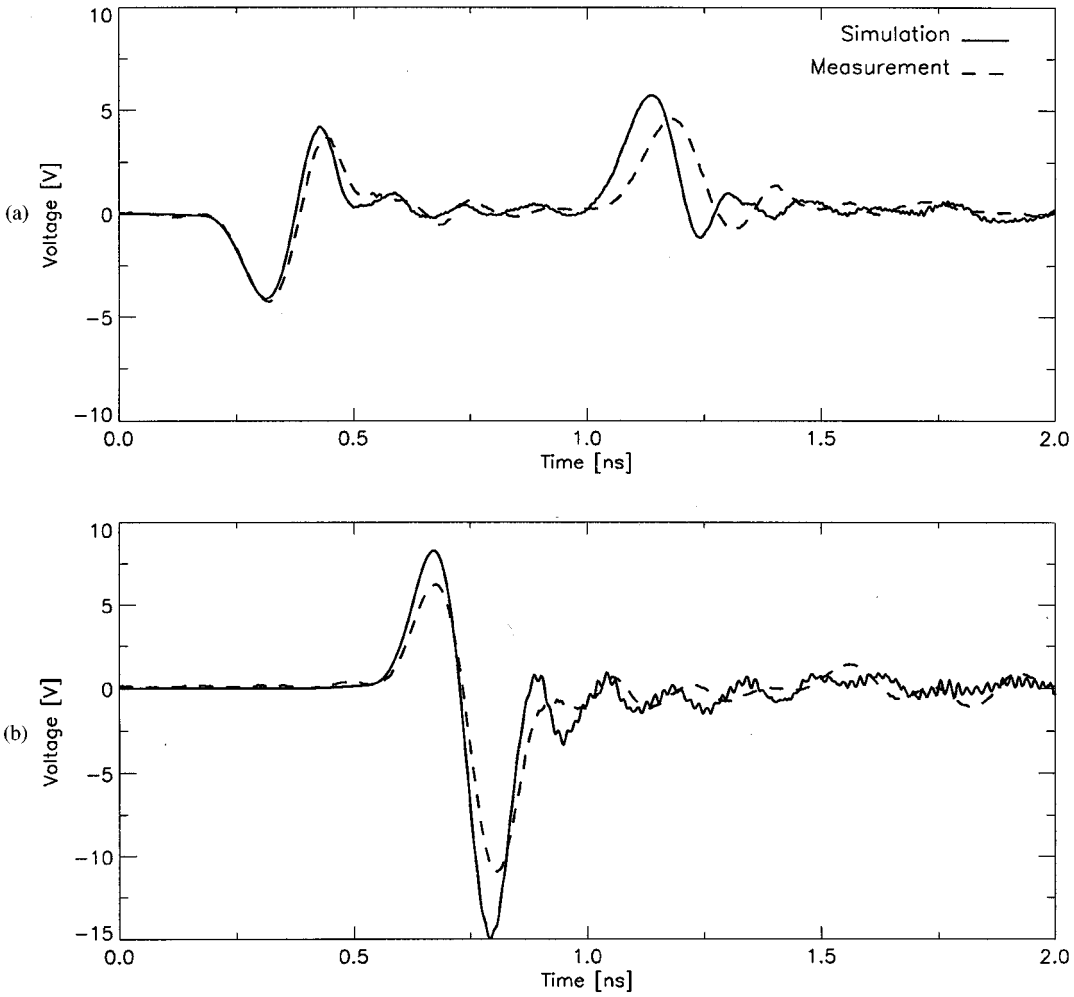

Fig. 11. Numerical simulation of the field to TL coupling with forward-biased diode at (a) the near end and (b) the far end; matched loads.

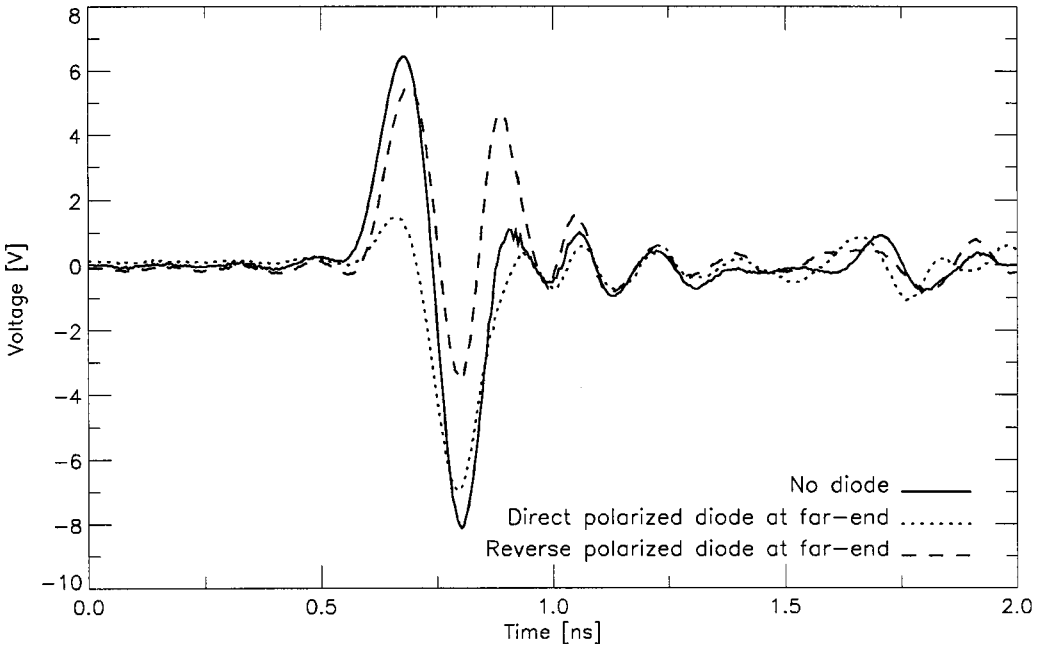

Fig. 12. Far-end measurements when the diode was placed at the far end of a two-conductor TL.

diamond-shaped cells shown in the figure. For the case of the PCB's considered herein the 2-D FDTD space was discretized, as shown in Fig. 7. Only two FDTD cells were used to model the thickness of the duroid dielectric substrate. Simple first-order absorbing boundary conditions were used and the incident tangential electric field $E_z(t)$ was imposed on the left-side boundary.

The measured field values (Fig. 4) were used as the excitation waveform. The calculated field values inside the substrate were output and stored in a database. The vertical boundaries were placed far from the substrate boundaries in order to assure that no reflections were picked up.

C. Incorporating Surface Waves into the Field-Coupling Mechanism

As the first case study, we choose the simple microstrip structure of Fig. 5(a) without the diode. The total modeled length of the strip is 99 mm and the approximate speed of the quasi-TEM wave propagating in such a line is calculated as $v_0 \cong 2.185 \times 10^8$ m/s. For the MTL modeling using (5), the line was divided into $K = 227$ cells, that is $\Delta y \cong 0.436$ mm. The time-step was chosen at the Courant limit of the numerical scheme, $\Delta t = \Delta y/v_0 = 1.996$ ps, which is sufficiently small to resolve the quasi-Gaussian pulse shown in Fig. 4 (more than 45 time samples in the main part of the pulse). The lumped element circuit, which was used to model the near-end and far-end of the line are shown in Fig. 8. In these circuits, $R_{\text{near}} = R_{\text{far}} = 50\ \Omega$ represent the impedance of the SMA connectors from which the induced signal was measured, $C\Delta y/2$ represents one half of the Π cell of the discretized TL, I_{f_0} and I_{f_K} represent currents induced by the incident plane wave. The current sources $I_{1/2}^{n+1/2}$ and $I_{K-1/2}^{n+1/2}$ represent discretized transmission-line (TL) currents, which are calculated using (5). The discretized voltages V_0 and V_K are calculated using MNA analysis [18].

Simulation results obtained assuming a pure plane wave model for the incident field, that is using (9), are shown in Fig. 9 and denoted as "without surface wave." Results obtained using the 2-D FDTD analysis described previously to simulate a more accurate incident field and then using (10) and (11) to model the distributed source terms are denoted "with surface wave" in the figure. Measured results are also shown. There are several differences between the waveforms. The amplitudes of the plane wave voltage waveforms are quite different from the other two waveforms shown in the figure and this is mostly due to the fact that the plane wave model does not account for the permittivity of the dielectric substrate. This also produces a propagation time difference. The most critical difference is the "inversion of polarity" that exists between the plane wave results and the measured waveform at the far-end of the TL. Using the 2-D FDTD simulation to more accurately model the perturbation of the incident field by the dielectric; that is, inclusion of the surface wave produces much better results.

The existence of the surface wave contributes to the apparance of the two voltage pulses at the far-end of the TL. The accuracy of this interpretation is confirmed by the results shown in Fig. 10. In this figure, measurements of the far-end voltages for the microstrip structures [Fig. 5(a)] with various dielectric substrate materials are shown.

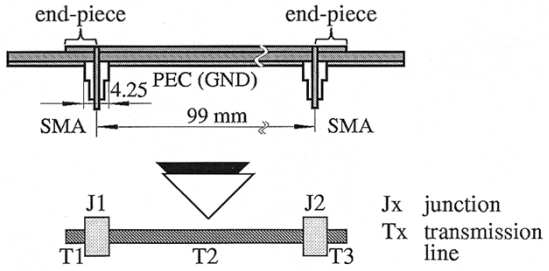

Fig. 13. Refined three-piece model of line.

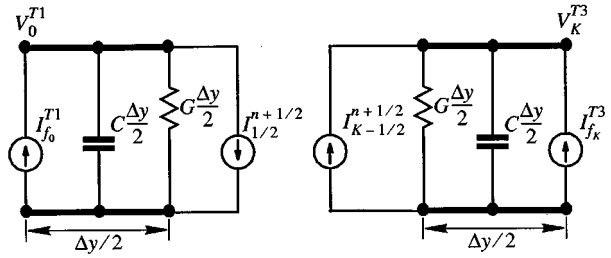

Fig. 14. Lumped-element models of the near- and far-end termination circuits.

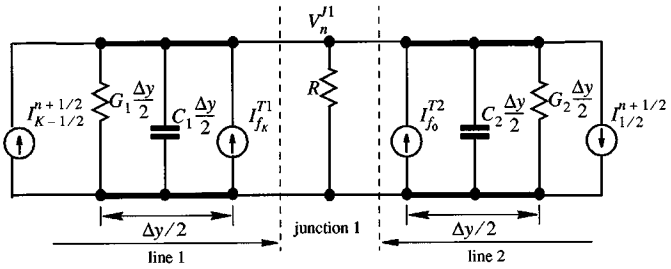

Fig. 15. The linear junction between two Π-modeled two-conductor lossy TL's.

When the permittivity of the substrate material is increased the surface wave effect becomes more noticeable and we see the two voltage pulses separately. The dielectric constant of the test case denoted "high dielectric" in the figure is $\varepsilon_r \cong 4.5 \pm 0.045$ [TMM-4 material (see footnote 2)], whereas that of the foam is $\varepsilon_r \cong 1.05$. In this case, the two waveforms are separated by a greater time than for the duroid case.

In all test cases, using the more accurate model for the field-to-MTL coupling was required to get good results that matched the experimental data well. This required the calculation of the incident fields and voltages using the 2-D FDTD simulation in conjunction with (10) and (11). In all the remaining results that are reported in this paper, this is the technique that is used.

D. Nonlinear Termination

Several configurations were studied in which a diode was placed at either the near end or the far end of the TL. Fig. 11 depicts the measured and simulated results of the near- and far-end voltages for the case of a forward-biased diode placed at the near end of the single microstrip line shown in Fig. 5(a). Notice, by comparing Figs. 9 and 11, that the effect of the diode

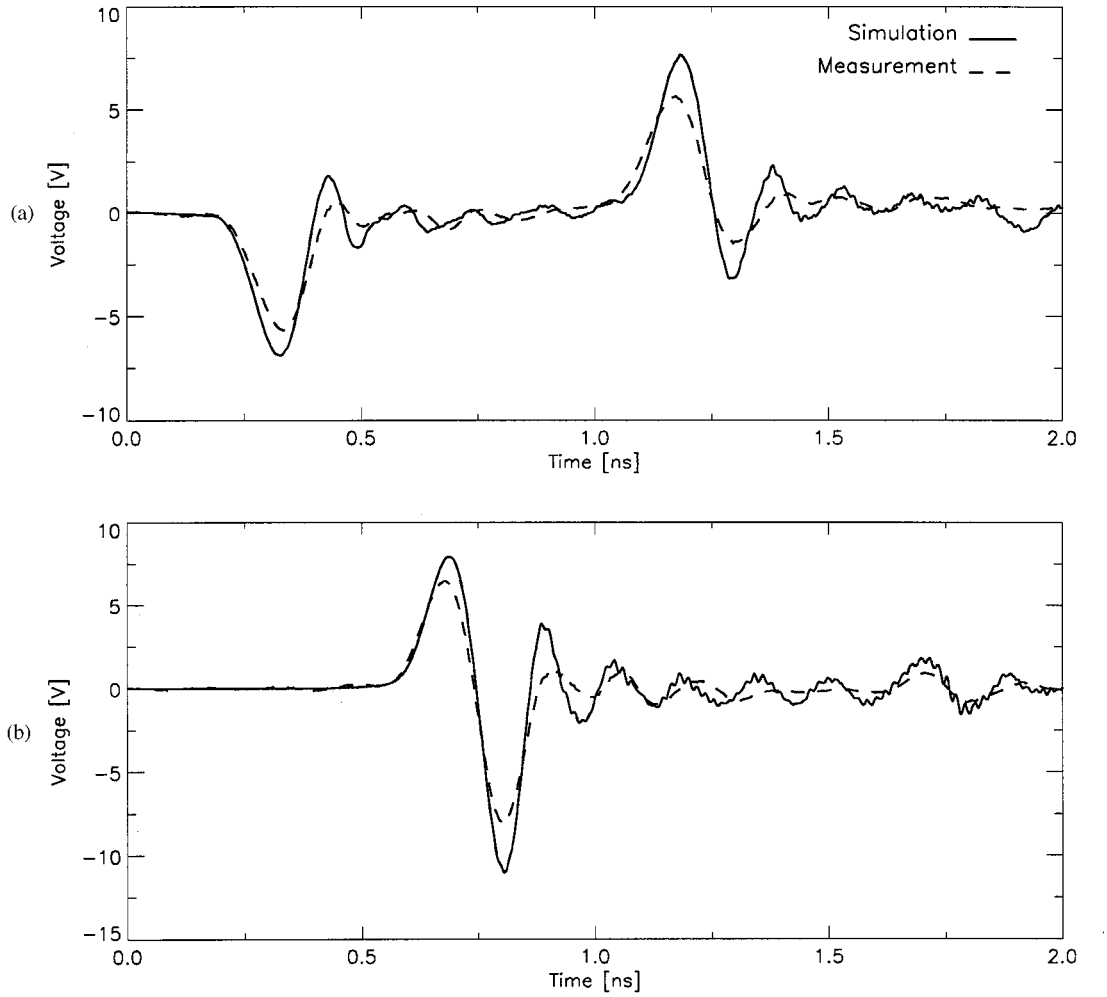

Fig. 16. Three-piece model with matched loads. (a) Near end. (b) Far end.

is to slightly reduce the peak-value of the near-end voltage, to introduce a new positive peak and to increase the peak-value of the far-end voltage. The approximate junction capacitance of 1 pF of the diode is not negligible and it was taken into account in the numerical simulations in the form of a lumped capacitance connected in parallel with a purely resistive junction diode modeled by the well-known formula

$$I = I_o(e^{V_D/V_T} - 1) \tag{12}$$

where $V_T = 26$ mV was used and V_D is the voltage across the diode. The voltages measured at the far-end when the diode was also placed at the far end are shown in Fig. 12. The three cases of no diode, forward biased diode, and a reverse biased diode are shown.

E. Three-Piece Microstrip Models

The slight delays in the propagation of pulses in the simulations as compared to the measured results implies that the length of the line is not modeled properly. Therefore, a "three-piece" model of the microstrip structure was introduced in which the "overhangs" (see Fig. 13) of the conductors above the SMA connectors are modeled as two open-ended TL's (T1 and T3). These overhangs or "end pieces," are connected to the two ends of the main line via two lumped element junctions (J1 and J2). The equivalent lumped element circuit models of the open ends of T1 and T3 are shown in Fig. 14, whereas an example of the lumped element model for junction J1 is shown in Fig. 15.

The three-piece model results match the experimental results better in terms of the timing of the individual pulses, but the amplitudes are worse than the one-piece model. Near- and far-end voltage results for a single line with no diode are shown in Fig. 16. Results for the case of a forward-biased diode placed at the near end of the single microstrip are shown in Fig. 17. These can be compared to the one-piece results for the same test shown in Figs. 9 and 11.

For the latter nonlinear case (Fig. 17), the time step used was $\Delta t = 1.5845$ ps. The end-piece TL's were resolved into 13 cells each with $\Delta y_{\text{end-pieces}} = 0.346$ mm and the leapfrog scheme was run at the Courant limit. Two more TL's were required (one from each SMA connector to the surface mount diode): a short line with seven cells of size $\Delta y = 0.357$ mm and a long TL

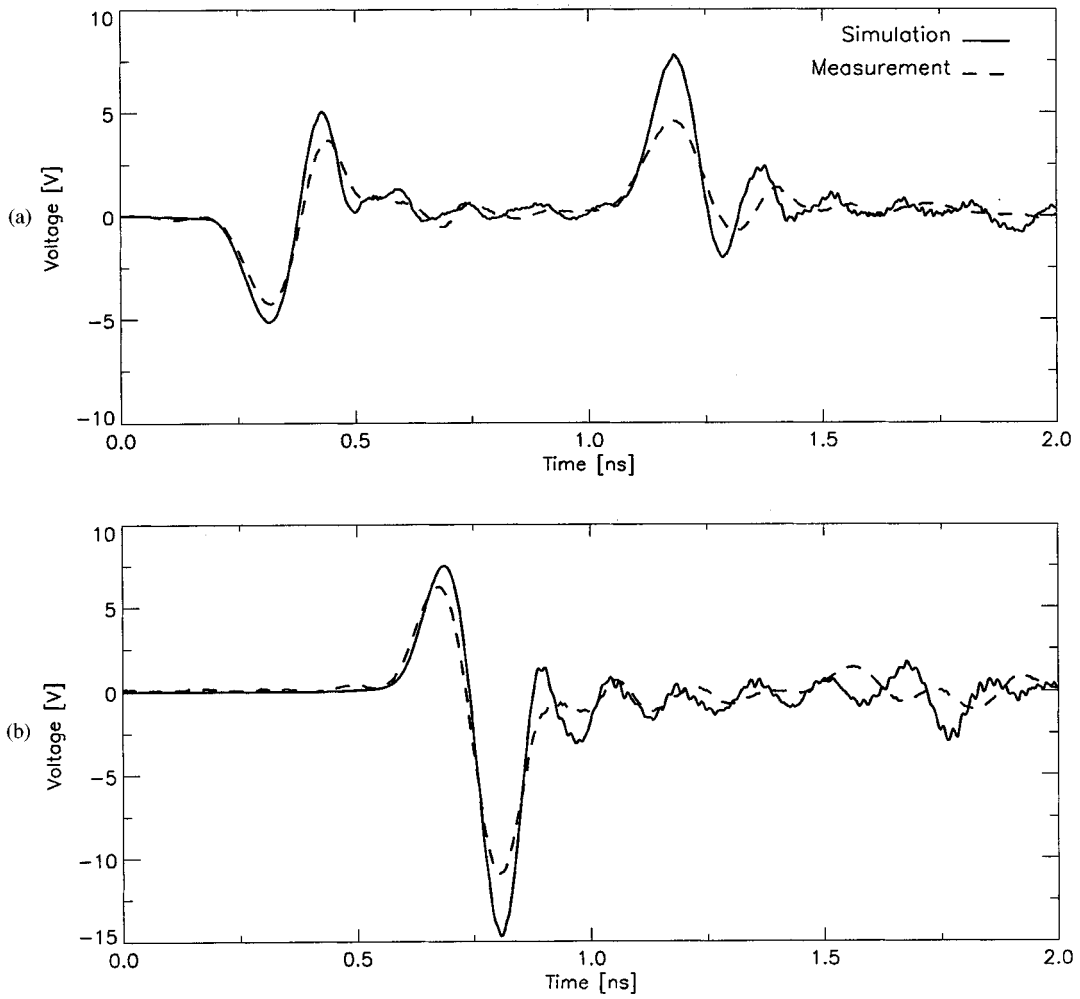

Fig. 17. Three-piece model with forward-biased diode at near-end and "matched" loads. (a) Near end. (b) Far end.

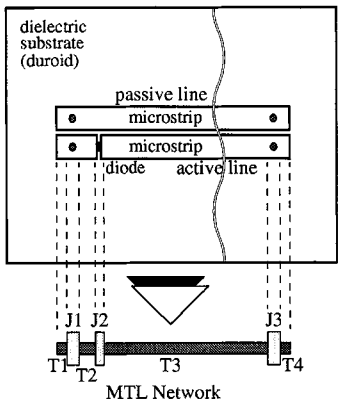

Fig. 18. MTL network of the coupled microstrip problem.

with 275 cells of size $\Delta y = 0.347$ mm. Since the time-step of the algorithm must remain the same for all TL's, the update equations for these center two lines were run at Courant numbers $v_0 \Delta t / \Delta y$ of 0.969 and 0.996, respectively.

Similar experiments were carried out with coupled microstrips shown in Fig. 5(b). It is well known that the matching load of an MTL is a "matrix" impedance network. In the measurements, the same SMA "probes" were used without any additional components. Therefore, the termination network did not meet the MTL matching criteria and the lines were only partially matched. In the numerical simulations for this case, four three-conductor multiconductor TL's (T1, T2, T3, and T4) forming a network as shown in Fig. 18 were used. TL's T1 and T4 model the end pieces, junctions J1 and J3 model the SMA connectors, and junction J2 models the surface-mount diode. Results of simulations and experiment are shown in Fig. 19. As can be seen from these plots, except for a small difference in magnitude, the simulation results are in excellent agreement with the experimental measurements. It is worth mentioning that in these nonlinear cases, the diode's own junction capacitance of approximately 1 pF essentially suppresses the nonlinear characteristics of the diode itself, which is why we do not see more of a rectifying effect.

VI. Conclusions

The numerical prediction of the induced voltages and currents due to an external field coupling to a printed

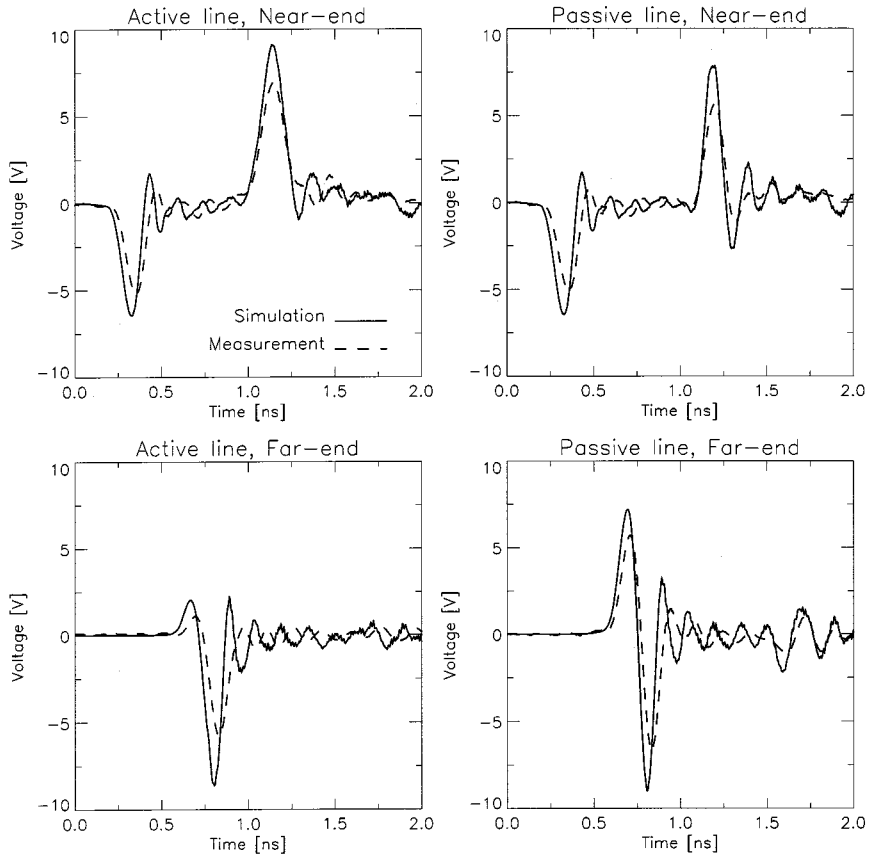

Fig. 19. Coupled microstrip: duroid substrate three-conductor TL with a forward-biased diode at the far end in the active line. (All ends terminated in 50-Ω SMA connectors.)

MTL network with nonlinear components at the junctions has been considered. The modeling method is based on finite-difference solutions of the quasi-TEM MTL equations and MNA formulation of the junctions in the network. The experimental validation of these MTL network models is a fairly complicated task since it involves the treatment of several possible sources of error. Making accurate field measurements, for instance, is just as demanding as finding a good numerical model for the network. The test cases considered herein show the importance of accurately modeling the incident electromagnetic field in the proximity of the TL's. It was shown that the perturbation of the incident plane wave caused by the dielectric substrate of a PCB is an important factor which must be accounted for in the MTL models. As a result, the simple and efficient, but purely plane wave coupling models that have been used in the past are inadequate. It was shown that for the end-fire incidence case considered herein, a simple 2-D FDTD field simulation sufficiently characterized the incident field including the surface wave, which arises due to the air-dielectric interface of the circuit board. For more complicated dielectric substrates and/or incident fields, a 3-D numerical field simulation would be required. The amount of memory needed to store such a time-domain field simulation is of concern, especially if this technique is to be applied to large circuits, but the field simulation would only have to be performed once even when the MTL network topology would change.

REFERENCES

[1] M. Picket-May, A. Taflove, and J. Baron, "FDTD modeling of digital signal propagation in 3-D circuits with passive and active loads," *IEEE Trans. Microwave Theory Tech.*, vol. 42, pp. 1514–1523, Aug. 1994.

[2] Y.-S. Tsuei, A. C. Cangellaris, and J. L. Prince, "Rigorous electromagnetic modeling of chip-to-package (first-level) interconnections," *IEEE Trans. Comput. Hybrids, Manufact. Technol.*, vol. 16, pp. 876–883, Dec. 1993.

[3] W. Pinello, A. C. Cangellaris, and A. Ruehli, "Hybrid electromagnetic modeling of noise interactions in packaged electronics based on the partial-element equivalent-circuit formulation," *IEEE Trans. Microwave Theory Tech.*, vol. 45, pp. 1889–1896, Oct. 1997.

[4] C. R. Paul, *Analysis of Multiconductor Transmission Lines—Series in Microwave and Optical Engineering*, New York: Wiley, 1994.

[5] T. K. Tang, M. S. Nakhla, and R. Griffith, "Analysis of lossy multiconductor transmission lines using the asymptotic waveform evaluation technique," *IEEE Trans. Microwave Theory Tech.*, vol. 39, pp. 2107–2116, Dec. 1991.

[6] D. Lee and O. A. Palusinski, "Adaptation of 'SPICE3' to simulation of lossy multiple-coupled TLs," *IEEE Trans. Comput., Packaging, Manufact. Tech.—Part B: Adv. Packaging.*, vol. 17, pp. 125–133, May 1994.

[7] I. Maio, F. G. Canavero, and B. Dilecce, "Analysis of crosstalk and field coupling to lossy MTL's in a Spice environment," *IEEE Trans. Electromagn. Compat.*, vol. 38, pp. 221–229, Aug. 1996.

[8] M. Celik, C. A. Cangellaris, and A. Yaghmour, "An all-purpose transmission-line model for interconnect simulation in Spice," *IEEE Trans. Microwave Theory Tech.*, vol. 45, pp. 1857–1867, Oct. 1997.

[9] C. D. Taylor, R. S. Satterwhite, and C. W. Harrison Jr., "The response of a terminated two wire transmission lines excited by a nonuniform electromagnetic field," *IEEE Trans. Antennas Propagat.*, vol. 13, pp. 987–989, Nov. 1965.

[10] A. K. Agrawal, H. J. Price, and S. H. Gurbaxani, "Transient response of multiconductor transmission lines excited by a nonuniform electromagnetic field," *IEEE Trans. Electromagn. Compat.*, vol. EMC-22, pp. 119–129, May 1980.

[11] F. Rachidi, "Formulation of field to TL coupling equations in terms of magnetic excitation," *IEEE Trans. Electromagn. Compat.*, vol. 35, pp. 404–407, Aug. 1993.
[12] I. Maio and F. G. Canavero, "Transient field coupling and crosstalk in lossy lines with arbitrary loads," *IEEE Trans. Electromagn. Compat.*, vol. 37, pp. 599–606, Nov. 1995.
[13] P. Bernardi and R. Cicchetti, "Response of a planar microstrip line excited by an external electromagnetic field," *IEEE Trans. Electromagn. Compat.*, vol. 32, pp. 98–105, May 1990.
[14] P. Bernardi, R. Cicchetti, and D. S. Moreolo, "A full-wave model for EMI prediction in planar microstrip circuits excited in the near-field of a short electric dipole," *IEEE Trans. Electromagn. Compat.*, vol. 37, no. 2, pp. 175–182, May 1995.
[15] S. A. Podosenov and A. A. Sokolov, "Linear two-wire TL coupling to an external electromagnetic field—Part I: Theory," *IEEE Trans. Electromagn. Compat.*, vol. 37, pp. 559–566, Nov. 1995.
[16] S. A. Podosenov, K. Yu. Sakharov, Ya. G. Svekis, and A. A. Sokolov, "Linear two-wire TL coupling to an external electromagnetic field—Part II: Specific cases, experiment," *IEEE Trans. Electromagn. Compat.*, vol. 37, pp. 566–574, Nov. 1995.
[17] S. Tkatchenko, F. Rachidi, and M. Ianoz, "Electromagnetic field coupling to a line of finite length: Theory and fast iterative solutions in frequency and time domains," *IEEE Trans. Electromagn. Compat.*, pp. 509–518, Nov. 1995.
[18] D. Mardare and J. LoVetri, "The finite-difference time-domain solution of lossy MTL networks with nonlinear junctions," *IEEE Trans. Electromagn. Compat.*, vol. 37, pp. 252–259, May 1995.
[19] J. Vlach and K. Singhal, *Computer Methods for Circuit Analysis and Design*, 2nd ed. ed. New York: Van Nostrand Reinhold, 1994.
[20] K. S. Kunz and R. J. Luebbers, *The Finite Difference Time Domain Method for Electromagnetics*. Boca Raton, FL: CRC, 1993.
[21] A. C. Cangellaris, "Distributed equivalent sources for the analysis of multiconductor TLs excited by an electromagnetic field," *IEEE Trans. Microwave Theory Tech.*, vol. 36, pp. 1445–1448, Oct. 1988.

Tibor Lapohos (S'93–M'98) was born in Tîrgu-Mures, Romania, in 1967. He received the E.E. degree from the Department of Automation and Computer Technology of the Polytechnic University, Cluj-Napoca, Romania, in 1991, and the M.E.Sc. and Ph.D. degrees from the University of Western Ontario, Canada, in 1994 and 1998, respectively.

In 1998, he joined the Electronic Countermeasures Section of the Defence Research Establishment Ottawa, Canada, as a Defence Scientist. His main areas of interest are in wide-band sensors, time-domain measurements, electromagnetic compatibility problems, and time-domain numerical methods. He is also interested in artificial intelligence.

Joe LoVetri (S'84–M'90) was born in Enna, Italy, in 1963. He received the B.Sc. (with distinction) and M.Sc. degrees, both in electrical engineering, from the University of Manitoba, Canada, in 1984 and 1987, respectively, and the Ph.D. degree in electrical engineering from the University of Ottawa, Canada, in 1991.

From 1984 to 1986, he was an EMI/EMC Engineer at Sperry Defence Division, Winnipeg, Manitoba, Canada. From 1986 to 1988 he held the position of TEMPEST Engineer at the Communications Security Establishment, Ottawa, Canada. From 1988 to 1991 he was a Research Officer at the Institute for Information Technology of the National Research Council of Canada. From 1991 to 1999 he was an Associate Professor in the Department of Electrical and Computer Engineering, University of Western Ontario. From 1997 to 1998 he spent a sabbatical year at the TNO Physics and Electronics Laboratory, The Netherlands. He is currently with the Department of Electrical and Computer Engineering, University of Manitoba. His main interests are in time-domain computational electromagnetics, modeling of electromagnetic compatibility problems, ground-penetrating radar, and wide-band identification techniques.

Joe Seregelyi (M'95) was born in Welland, Canada, on October 10, 1962. He received the B.Eng. and M.Eng. degrees in engineering physics from McMaster University, Canada, in 1985 and 1988, respectively.

From 1988 to 1993, he was a Research Scientist at the National Research Council of Canada. Currently, he is employed by the EMC Group, Communications Research Centre, Ottawa, Canada, and is partially seconded to the Defence Research Establishment Ottawa. He has extensive experience in several areas of electromagnetic and electrooptic design and measurement. His current interests include generation of standard electromagnetic fields, design of field sensors, detection and neutralization of landmines, electromagnetic effects in biological systems and devices, and ultrawide-band radar systems.

Mr. Seregelyi is a Registered Professional Engineer in Ontario, Canada.